

c.2



# Lawrence Berkeley Laboratory

UNIVERSITY OF CALIFORNIA

## EARTH SCIENCES DIVISION

RECEIVED  
LIBRARY AND  
DOCUMENTS SECTION  
BERKELEY LABORATORY

JUN 9 1988

LIBRARY AND  
DOCUMENTS SECTION

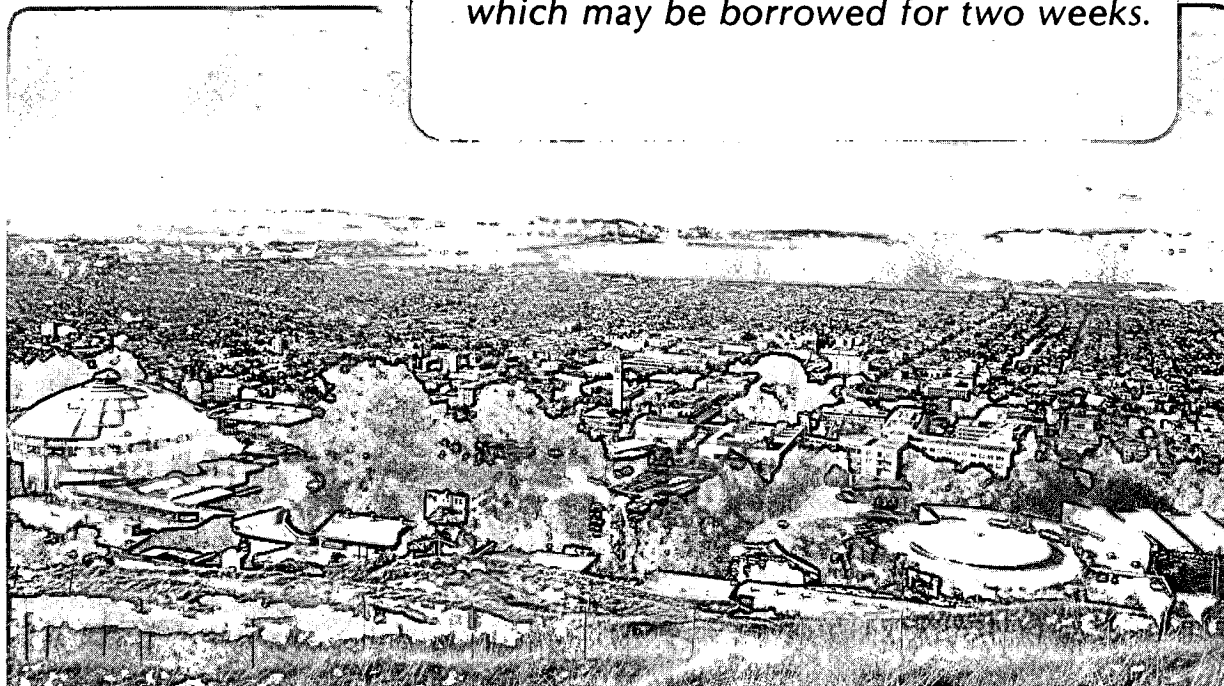
### Steady-State Radionuclide Transfer from a Cylinder Intersected by a Fissure

S.J. Zavoshy, P.L. Chambré, J. Ahn,  
T.H. Pigford, and W.W.-L. Lee

March 1988

**TWO-WEEK LOAN COPY**

*This is a Library Circulating Copy  
which may be borrowed for two weeks.*



LBL-23986  
c.2

## **DISCLAIMER**

This document was prepared as an account of work sponsored by the United States Government. While this document is believed to contain correct information, neither the United States Government nor any agency thereof, nor the Regents of the University of California, nor any of their employees, makes any warranty, express or implied, or assumes any legal responsibility for the accuracy, completeness, or usefulness of any information, apparatus, product, or process disclosed, or represents that its use would not infringe privately owned rights. Reference herein to any specific commercial product, process, or service by its trade name, trademark, manufacturer, or otherwise, does not necessarily constitute or imply its endorsement, recommendation, or favoring by the United States Government or any agency thereof, or the Regents of the University of California. The views and opinions of authors expressed herein do not necessarily state or reflect those of the United States Government or any agency thereof or the Regents of the University of California.

LBL-23986  
UCB-NE-4113  
UC-70

**STEADY-STATE RADIONUCLIDE TRANSFER FROM A  
CYLINDER INTERSECTED BY A FISSURE**

**S. J. Zavoshy, P. L. Chambré, J. Ahn, T. H. Pigford and W. W-L. Lee**

**Earth Sciences Division, Lawrence Berkeley Laboratory**

**and**

**Department of Nuclear Engineering**

**University of California**

**Berkeley, CA 94720**

**March 1988**

---

Work supported in part by U. S. Department of Energy contract DE-AC03-76SF00098

The authors invite comments and would appreciate being notified of any errors in the report.

T. H. Pigford  
Department of Nuclear Engineering  
University of California  
Berkeley, CA 94720

### ACKNOWLEDGEMENT

**This research was supported in part by the U. S. Department of Energy, Office of Civilian Radioactive Waste Management, Repository Technology Program. The conclusions of the authors are not necessarily endorsed or approved by the U. S. Department of Energy.**

## CONTENTS

<b>1. Introduction</b> . . . . .	<b>1</b>
<b>2. Review of Past Work</b> . . . . .	<b>3</b>
<b>3. Governing Equations</b> . . . . .	<b>5</b>
<b>4. Steady-State Analysis</b> . . . . .	<b>6</b>
<b>4.1 Mass Flux Derivations</b> . . . . .	<b>14</b>
<b>4.2 Numerical Demonstrations</b> . . . . .	<b>15</b>
<b>4.2.1 Method of Evaluation</b> . . . . .	<b>15</b>
<b>4.2.2 Numerical Results</b> . . . . .	<b>17</b>
<b>5. Conclusions</b> . . . . .	<b>30</b>
<b>6. References</b> . . . . .	<b>32</b>

## TABLE

Table 1. Values of $\beta_1$ and $\beta_2$ for some radionuclides of interest . . . . .	19
---	----

## FIGURES

Figure 1. Schematic representation of a waste cylinder intersected by a fissure . . . . .	4
Figure 2. Variation of normalized concentration with $r/a$ for different $a/b$ ratios . . . . .	18
Figure 3. Variation of normalized concentration with $r/a$ for different retardation coefficients . . . . .	21
Figure 4. Variation of normalized concentration with $r/a$ for different Thiele ( $\lambda$ ) values . . . . .	22
Figure 5. Variation of normalized concentration with $z/b$ for $a/b=15$ . . . . .	23
Figure 6. Variation of normalized flux with $z/b$ for different $a/b$ ratios . . . . .	26
Figure 7. Ratio of mass flux in the radial direction to that in the axial direction at the rock/fissure interface . . . . .	27
Figure 8. Variation of mass loss rate from a waste cylinder with retardation coefficient . . . . .	28

# STEADY-STATE RADIONUCLIDE TRANSFER FROM A CYLINDER INTERSECTED BY A FISSURE<sup>1</sup>

## 1. Introduction

In a geologic repository of nuclear waste in crystalline rock, it may be necessary to emplace a waste package across a fissure or fracture. Because these fissures may be preferential pathways for radionuclide migration, it is important to investigate the effect of fractures in a porous rock on the rate of mass transfer of radionuclides from a waste cylinder. Previous investigators assumed that:

- (1) The nuclide diffuses in the fissure.
- (2) The nuclide concentration in the fissure is uniform in the transverse direction, i.e., parallel to the waste cylinder axis.
- (3) In the porous rock, the nuclide diffuses only in the transverse direction, i.e., parallel to the waste cylinder axis.

Such a formulation does not include mass transfer at the waste/rock interface. Our intent is to investigate the problem more fully.

Section 2 is a review of previous work.

In Section 3, we give the governing equation for mass transport of radionuclides from a waste cylinder intersected by a planar fissure. We assume that mass transport is due to molecular diffusion in the water content of fissure and porous rock only. Here, we explicitly consider the nuclide diffusion in the longitudinal and transverse

---

<sup>1</sup>Adapted from Chapter 5 of S. J. Zavoshy's Ph.D. dissertation, Chairperson P. L. Chambré.

directions in the fissure as well as in the porous rock. This formulation permits us to investigate the validity of simplifying assumptions made by other investigators.

In Section 4, We give the analytical solution for the steady-state case. Numerical results indicate that for a waste radius of 15 cm and fissure width of 1 cm the concentration at the fissure/rock interface is 99.9 percent of the concentration at the fissure's center line. We also evaluate mass flux, surface mass flux, and mass flux integrated over the surface of the waste cylinder. We demonstrate the above quantities for several radionuclides of interest. Data show that surface mass flux increases as the radioactive decay constant and/or the retardation coefficient increases. Furthermore, for a waste glass cylinder with a height of 240 cm three times more mass is lost from the waste cylinder to the porous rock than from the waste cylinder to the fissure.

Section 5 states the conclusion of this analysis with the following observations:

- (1) The results of exact formulation in Section 4 indicate that the concentration of the diffusing nuclide in the fissure is almost uniform in the transverse direction, i.e., parallel to the cylinder axis; hence, one can use a simplified model by assuming a uniform concentration in the fissure in the transverse direction.
- (2) Radial diffusion in the porous rock is important and should be included in any mass transport analysis for a waste cylinder intersected by a fissure. Our data show that for a fissure width of 1 cm and waste cylinder height of 240 cm, almost 3 times more mass is lost from the waste cylinder to the porous rock than is lost to the fissure.

## 2. Review of Past Work

Figure 1 shows a schematic representation of the problem. The waste cylinder is idealized as an infinitely long cylinder and the fracture is assumed to be perpendicular to the cylinder axis. Previous investigators [1], [2], section 5 in Ref. [3], [4], [5], considered a slab which is intersected by a fissure and made the following simplifications:

- (1) The concentration of the nuclide in the fissure is uniform in the transverse ( $z$ ) direction.
- (2) Nuclides diffuse in the longitudinal (radial) direction in the fissure.
- (3) Nuclides do not diffuse in the longitudinal (radial) direction in the water-saturated porous rock.
- (4) Nuclides diffuse in the transverse ( $z$ ) direction in the water-saturated porous rock.

Reference [6] did not assume (1) and (2) above. From assumption (3) it follows that the mass transfer rate across the waste/porous rock interface is zero. This formulation leads to a representation of porous rock/waste interface as a diffusion barrier; thus decreasing the net rate of the waste dissolution.

The effect of parallel fractures on the mass transport rate was analyzed [7]. It was concluded that porous rock acts less as a sink for parallel fractures than for a single fracture. Because the rock between the fissures is of a finite thickness and hence has a finite capacity as a nuclide sink.

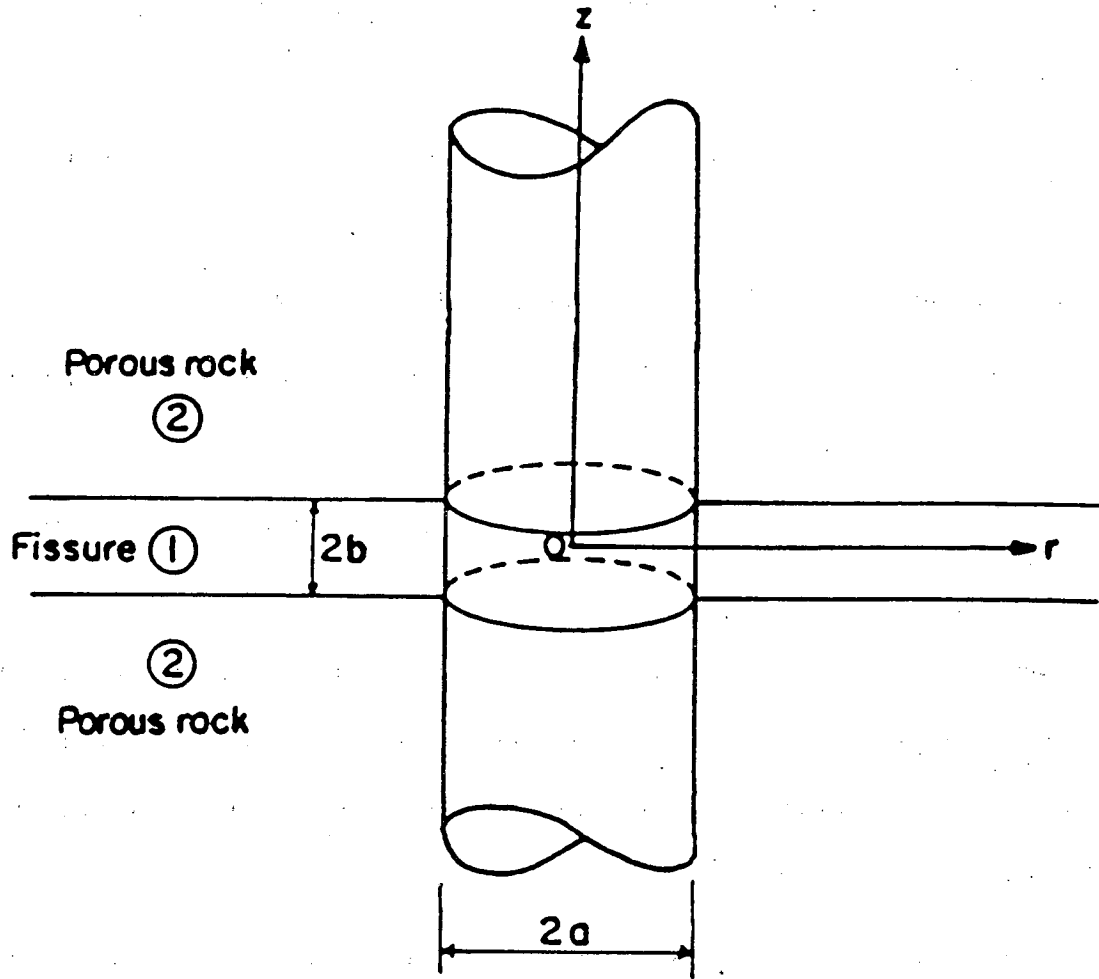


Figure 1 Schematic representation of a waste cylinder intersected by a fissure.

### 3. Governing Equations

The purpose of this research is to investigate the effect of a fracture in porous rock on the rate of mass transfer of radionuclides from a waste cylinder. Figure 1 shows a schematic of the problem. The waste cylinder is idealized as an infinitely long cylinder and the fracture is assumed to be perpendicular to the cylinder axis. Mass transfer is assumed to be due to molecular diffusion only. Subscript 1 indicates a fissure and subscript 2 indicates a water-saturated porous rock.

The governing equation for a radionuclide without precursor is given by:

$$K_i \frac{\partial N_i(r, z, t)}{\partial t} = \frac{D_i}{r} \frac{\partial}{\partial r} \left( r \frac{\partial N_i(r, z, t)}{\partial r} \right) + \quad (1)$$

$$+ D_i \frac{\partial^2 N_i(r, z, t)}{\partial z^2} - \lambda K_i N_i(r, z, t)$$

$$\text{for } i=1 \quad t > 0, r > a, 0 \leq z < b; \text{ for } i=2 \quad t > 0, r > a, b < z < \infty$$

where  $K_i$  is the retardation coefficient in region  $i$  ( $K_1=1$ ),  $N_i(r, z, t)$  is the concentration of radionuclide in ground water in region  $i$ ,  $\text{g/cm}^3$ ;  $D_i$  is the molecular diffusion coefficient of the radionuclide in the region  $i$ ,  $\text{cm}^2/\text{sec}$ ;  $\lambda$  is the decay constant,  $1/\text{sec}$ ;  $a$  is the cylinder radius,  $\text{cm}$ ;  $b$  is the fissure half-width,  $\text{cm}$ ;  $r$  is the radial position,  $\text{cm}$ ;  $z$  is the axial position,  $\text{cm}$ ; and  $t$  is time,  $\text{sec}$ .

To solve the equation we require initial and boundary conditions. The initial condition is given by

$$N_i(r, z, 0) = 0 \quad , i=1 \quad a < r < \infty, 0 \leq z \leq b; \quad i=2 \quad a < r < \infty, b \leq z < \infty \quad (2)$$

Equation (2) indicates that initially the concentration of the radionuclide in the water in the fissure as well as the porous rock is zero. Note that we have used symmetry with respect to the plane  $z=0$  to write the initial condition for the range

$0 \leq z \leq \infty$ . The boundary conditions are

$$N_i(a, z, t) = N^* \quad , i=1, 0 \leq z \leq b, t > 0; \quad i=2, b \leq z < \infty, t > 0 \quad (3)$$

$$N_i(\infty, z, t) = 0 \quad , i=1, 0 \leq z \leq b, t > 0; \quad i=2, b \leq z < \infty, t > 0 \quad (4)$$

$$\frac{\partial N_1(r, 0, t)}{\partial z} = 0 \quad , r > a, t > 0 \quad (5)$$

$$\frac{\partial N_2(r, \infty, t)}{\partial z} = 0 \quad , r > a, t > 0 \quad (6)$$

$$N_1(r, b, t) = N_2(r, b, t) \quad , r > a, t > 0 \quad (7)$$

$$-D_1 \frac{\partial N_1(r, b, t)}{\partial z} = -\epsilon D_2 \frac{\partial N_2(r, b, t)}{\partial z} \quad , r > a, t > 0 \quad (8)$$

Here  $N^*$  is the saturation concentration of the nuclide in ground water,  $\text{g/cm}^3$ , and  $\epsilon$  is the porosity of the porous rock. Equation (3) indicates that the concentration of the nuclide in the water adjacent to the waste surface is equal to  $N^*$ . Equation (4) indicates that the concentration of the nuclide in the water far away from the cylinder is equal to the initial concentration. Equation (5) indicates the symmetry of the problem with respect to the plane  $z=0$ . Equation (6) indicates that far away from the fissure the concentration becomes independent of  $z$ , i.e., the concentration is due to diffusion from the waste/rock interface only. Equations (7) and (8) indicate continuity of the concentration and mass flux across the fissure/rock interface. The left hand side of Eq.(8) does not have a porosity factor explicitly since the porosity of the fissure is unity.

#### 4. Steady-State Analysis

At steady-state  $\frac{\partial N_i(r, z, t)}{\partial t} = 0$ . As a short-hand notation we write  $N_1(r, z)$  and  $N_2(r, z)$  to indicate a steady-state solution. The governing equation (1) is writ-

ten as:

$$\frac{D_i}{r} \frac{\partial}{\partial r} \left( r \frac{\partial N_i(r, z)}{\partial r} \right) + D_i \frac{\partial^2 N_i(r, z)}{\partial z^2} - \lambda K_i N_i(r, z) = 0 \quad (9)$$

for  $i=1$   $r > a$ ,  $0 \leq z < b$ ; for  $i=2$   $r > a$ ,  $b < z < \infty$

The side conditions are given by:

$$N_i(a, z) = N^* \quad , \text{ for } i=1 \quad 0 \leq z \leq b; \text{ for } i=2 \quad b \leq z < \infty \quad (10)$$

$$N_i(\infty, z) = 0 \quad , \text{ for } i=1 \quad 0 \leq z \leq b; \text{ for } i=2 \quad b \leq z < \infty \quad (11)$$

$$\frac{\partial N_1(r, 0)}{\partial z} = 0 \quad , r > a \quad (12)$$

$$\frac{\partial N_2(r, \infty)}{\partial z} = 0 \quad , r > a \quad (13)$$

$$N_1(r, b) = N_2(r, b) \quad , r > a \quad (14)$$

$$-D_1 \frac{\partial N_1(r, b)}{\partial z} = -\epsilon D_2 \frac{\partial N_2(r, b)}{\partial z} \quad , r > a \quad (15)$$

The solution is obtained with the aid of the Weber transform. The Weber transform of  $f(r)$  is defined as  $\tilde{f}(p)$ ; the functional form is given by Eq.(S.1) in Ref. [8]:

$$\tilde{f}(p) \equiv \int_a^{\infty} f(r) W(r, p) r dr \quad (16)$$

where  $W(r, p)$  is defined as:

$$W(r, p) \equiv J_0(rp)Y_0(ap) - J_0(ap)Y_0(rp) \quad (17)$$

$J_0$  and  $Y_0$  are the Bessel functions of the first and second kind of order zero, respectively. For Eq.(16) to exist it is required that  $r^{\frac{1}{2}} f(r)$  to be integrable in the range  $0 < a \leq r \leq \infty$ , and  $p$  is positive. The inverse Weber transform is given by Eq.(S.3) in Ref. [8]:

$$f(r) = \int_0^{\infty} \tilde{f}(p) \frac{J_0(rp)Y_0(ap) - J_0(ap)Y_0(rp)}{[J_0(ap)]^2 + [Y_0(ap)]^2} p dp \quad (18)$$

Here we give some of the properties of Bessel functions (section 9.1, Eqs. 9.1.1, 9.1.1, 9.2.1, 9.2.2, 9.1.7, 9.1.8, 9.1.7, 9.1.9 9.1.28, 9.1.28, 9.1.60, 9.1.16 of Ref. [9] ; note that in Ref. [9] the argument is  $z$  which is a complex number and not the axial position  $z$ . Here, the argument is given in terms of the radial coordinate  $r$ ):

$$\frac{1}{r} \frac{\partial}{\partial r} \left( r \frac{\partial J_0(r)}{\partial r} \right) = -J_0(r) \quad (19)$$

$$\frac{1}{r} \frac{\partial}{\partial r} \left( r \frac{\partial Y_0(r)}{\partial r} \right) = -Y_0(r) \quad (20)$$

$$\lim_{r \rightarrow \infty} J_0(r) \approx \sqrt{\frac{2}{\pi r}} \left[ \cos\left(r - \frac{1}{4}\right) + O\left(\frac{1}{r}\right) \right] \quad (21)$$

$$\lim_{r \rightarrow \infty} Y_0(r) \approx \sqrt{\frac{2}{\pi r}} \left[ \sin\left(r - \frac{1}{4}\right) + O\left(\frac{1}{r}\right) \right] \quad (22)$$

$$\lim_{r \rightarrow 0} J_0(r) \approx 1 + O(r^2) \quad (23)$$

$$\lim_{r \rightarrow 0} \left[ Y_0(r) - \frac{2}{\pi} \ln(r) \right] \approx O(r^2) \quad (24)$$

$$\lim_{r \rightarrow 0} J_1(r) \approx 0 \quad (25)$$

$$\lim_{r \rightarrow 0} \left[ Y_1(r) + \frac{2}{\pi r} \right] \approx O(r) \quad (26)$$

$$\frac{d J_0(x)}{dx} = -J_1(x) \quad (27)$$

$$\frac{d Y_0(x)}{dx} = -Y_1(x) \quad (28)$$

$$J_n(x) \leq 1, \quad n=0,1 \quad (29)$$

$$J_1(x)Y_0(x) - J_0(x)Y_1(x) = \frac{2}{\pi x} \quad (30)$$

Using the above properties one can show that, ([10], Appendix C section 1.2, Eqs.(C.1)-(C.6)):

$$\frac{1}{r} \frac{\partial}{\partial r} \left( r \frac{\partial W(r,p)}{\partial r} \right) = -p^2 W(r,p) \quad (31)$$

$$W(a,p) = 0 \quad (32)$$

$$a \frac{\partial W(a,p)}{\partial r} = -\frac{2}{\pi} \quad (33)$$

$$\lim_{p \rightarrow \infty} [pf(p)W(r,p)] \approx 0 \quad \text{if } f(\infty) = 0 \quad (34)$$

Taking the Weber transform of Eq.(9) with respect to the radial coordinate  $r$ , integrating by parts with respect to  $r$ , changing the order of integration and differentiation with respect to  $z$  formally (assuming a finite  $z$ ), and using the above properties, we obtain ([10], Appendix C section 1.3, Eqs.(C.7)-(C.20)):

$$D_i \frac{d^2 \tilde{N}_i(z,p)}{dz^2} - \mu_i^2 \tilde{N}_i(z,p) - \frac{2}{\pi} D_i N^* = 0 \quad (35)$$

$$\text{for } i=1, 0 \leq z < b; \text{ for } i=2, b < z < \infty$$

where

$$\mu_i^2 \equiv p^2 D_i + \lambda K_i, \quad i=1,2 \quad (36)$$

$\mu_i$  is real since  $p$ ,  $D_i$ ,  $\lambda$ , and  $K_i$  are positive. The boundary conditions (12)-(15) are transformed to:

$$\frac{d\tilde{N}_1(p,0)}{dz} = 0 \quad (37)$$

$$\frac{d\tilde{N}_2(p,\infty)}{dz} = 0 \quad (38)$$

$$\tilde{N}_1(p,b) = \tilde{N}_2(p,b) \quad (39)$$

$$-D_1 \frac{d\tilde{N}_1(p,b)}{dz} = -\epsilon D_2 \frac{d\tilde{N}_2(p,b)}{dz} \quad (40)$$

The solution to Eqs.(35)-(40) is given by:

$$\begin{aligned} \bar{N}_1(p, z) &= A_1(p) \sinh\left(\frac{\mu_1 z}{\sqrt{D_1}}\right) + B_1(p) \cosh\left(\frac{\mu_1 z}{\sqrt{D_1}}\right) \\ &\quad - \frac{2 N^* D_1}{\pi \mu_1^2} \quad 0 \leq z \leq b \end{aligned} \quad (41)$$

$$\begin{aligned} \bar{N}_2(p, z) &= A_2(p) \exp\left(-\frac{\mu_2 z}{\sqrt{D_2}}\right) + B_2(p) \exp\left(\frac{\mu_2 z}{\sqrt{D_2}}\right) \\ &\quad - \frac{2 N^* D_2}{\pi \mu_2^2} \quad b \leq z < \infty \end{aligned} \quad (42)$$

From Eq.(37) it follows that  $A_1(p) \equiv 0$ . From Eq.(38) it follows that  $B_2(p) \equiv 0$  since  $\mu_2$  is positive.. From the remaining two boundary conditions we have that ([10], Appendix C section 1.4, Eqs.(C.21)-(C.27)):

$$B_1(p) = \frac{\frac{2 N^* D_1}{\pi \mu_1^2} - \frac{2 N^* D_2}{\pi \mu_2^2}}{\cosh\left(\frac{\mu_1 b}{\sqrt{D_1}}\right) + \frac{\mu_1}{\epsilon \mu_2} \left(\frac{D_1}{D_2}\right)^{\frac{1}{2}} \sinh\left(\frac{\mu_1 b}{\sqrt{D_1}}\right)} \quad (43)$$

$$A_2(p) = e^{-\frac{\mu_2 b}{\sqrt{D_2}}} \frac{-\frac{\mu_1}{\epsilon \mu_2} \left(\frac{D_1}{D_2}\right)^{\frac{1}{2}} \sinh\left(\frac{\mu_1 b}{\sqrt{D_1}}\right) \left[\frac{2 N^* D_1}{\pi \mu_1^2} - \frac{2 N^* D_2}{\pi \mu_2^2}\right]}{\cosh\left(\frac{\mu_1 b}{\sqrt{D_1}}\right) + \frac{\mu_1}{\epsilon \mu_2} \left(\frac{D_1}{D_2}\right)^{\frac{1}{2}} \sinh\left(\frac{\mu_1 b}{\sqrt{D_1}}\right)} \quad (44)$$

Before we proceed to take the inverse transform we consider the following auxiliary problem. The auxiliary problem will help us in obtaining partial inversion of inverse Weber transform of Eqs.(41) and (42). ([10], Appendix C section 1.5, Eqs.(C.30)-(C.33)):

$$\frac{D_i}{r} \frac{\partial}{\partial r} \left( r \frac{\partial N_i}{\partial r} \right) - \lambda K_i N_i = 0 \quad (45)$$

with the side conditions that:

$$N_i(a) = 1, \quad N_i(\infty) = 0 \quad (46)$$

The solution to this problem is  $\frac{K_0(\beta_i \frac{r}{a})}{K_0(\beta_i)}$ , where  $K_0$  is the modified Bessel function of

the first kind of the order zero [section 7.2, ref. 3], and  $\beta_i$  is defined as:

$$\beta_i^2 = \frac{\lambda K_i a^2}{D_i} \quad i=1,2 \quad (46A)$$

Some properties of  $K_0$  are given (Eqs.(9.6.27) and (9.7.2) of Ref.[9]):

$$\frac{d K_0(r)}{dr} = -K_1(r) \quad (46B)$$

$$\lim_{r \rightarrow \infty} [K_0(r)] \approx \sqrt{\frac{\pi}{2r}} e^{-r} \left[1 - \frac{1}{8r}\right] \quad (46C)$$

Now if we use the Weber transform on Eq.(45) we obtain that:

$$\tilde{N}_i(p) = -\frac{2}{\pi} \frac{D_i}{D_i p^2 + \lambda K_i} \quad (47)$$

Now taking the inverse transform and knowing the exact solution yields the following identity:

$$\frac{K_0(\beta_i \frac{r}{a})}{K_0(\beta_i)} \equiv \frac{-2}{\pi} \int_0^{\infty} \frac{J_0(rp) Y_0(ap) - J_0(ap) Y_0(rp)}{[J_0(ap)]^2 + [Y_0(ap)]^2} \frac{p dp}{p^2 + \frac{\lambda K_i}{D_i}} \quad r \geq a \quad (48)$$

Taking the inverse Weber transform yields  $N_1(r, z)$  and  $N_2(r, z)$ . The final result with the aid of identity (48) is: ([10], Appendix C section 1.6, Eqs.(C.34)-(C.36)):

$$N_1(r, z) = N^* \left[ \frac{K_0(\beta_1 \frac{r}{a})}{K_0(\beta_1)} - \frac{2}{\pi} \int_0^{\infty} \left( \frac{1}{p^2 + \frac{\lambda K_2}{D_2}} - \frac{1}{p^2 + \frac{\lambda}{D_1}} \right) \frac{J_0(rp) Y_0(ap) - J_0(ap) Y_0(rp)}{[J_0(ap)]^2 + [Y_0(ap)]^2} \frac{\cosh\left(\frac{\mu_1 z}{\sqrt{D_1}}\right) p dp}{\cosh\left(\frac{\mu_1 b}{\sqrt{D_1}}\right) + \frac{\mu_1}{\epsilon \mu_2} \left(\frac{D_1}{D_2}\right)^{\frac{1}{2}} \sinh\left(\frac{\mu_1 b}{\sqrt{D_1}}\right)} \right] \quad (49)$$

$$r \geq a, 0 \leq z \leq b$$

$$N_2(r, z) = N^* \left[ \frac{K_0(\beta_2 \frac{r}{a})}{K_0(\beta_2)} + \frac{2}{\pi} \int_0^\infty \left( \frac{1}{p^2 + \frac{\lambda K_2}{D_2}} - \frac{1}{p^2 + \frac{\lambda}{D_1}} \right) \right. \quad (50)$$

$$\frac{J_0(rp)Y_0(ap) - J_0(ap)Y_0(rp)}{[J_0(ap)]^2 + [Y_0(ap)]^2} \frac{\frac{\mu_1}{\epsilon\mu_2} \left(\frac{D_1}{D_2}\right)^{\frac{1}{2}} \sinh\left(\frac{\mu_1 b}{\sqrt{D_1}}\right)}{\cosh\left(\frac{\mu_1 b}{\sqrt{D_1}}\right) + \frac{\mu_1}{\epsilon\mu_2} \left(\frac{D_1}{D_2}\right)^{\frac{1}{2}} \sinh\left(\frac{\mu_1 b}{\sqrt{D_1}}\right)}$$

$$\left. \exp - \left[ \frac{\mu_2(z-b)}{\sqrt{D_2}} \right] p dp \right] , r \geq a, b \leq z < \infty$$

Before we proceed to verify that Eqs.(49) and (50) are the solutions to our problem we make some general observations. As  $b \rightarrow 0$ , waste is exposed to porous rock only. In this case the  $z$  domain of Eq.(49) vanishes and Eq.(50) with the aid of

Eq.(48) is reduced to  $N^* \frac{K_0(\beta_2 \frac{r}{a})}{K_0(\beta_2)}$ , which has been derived previously in section 7.2 of

[3]. On the other hand, if  $b \rightarrow \infty$  the waste is exposed to a water medium only. In

this case Eq.(50) vanishes and for any finite  $z$  Eq.(49) is simplified to  $N^* \frac{K_0(\beta_1 \frac{r}{a})}{K_0(\beta_1)}$ .

The terms in Eqs.(49) and (50) have the following significance: the first term indicates the concentration of a diffusing radionuclide if it was exposed to medium  $i$  only. The second term indicates the effect of a second medium on the concentration, i.e., perturbation of the concentration due to the other medium.

As a short-hand notation we introduce the following terms:

$$\Delta(p) \equiv \frac{1}{p^2 + \frac{\lambda K_2}{D_2}} - \frac{1}{p^2 + \frac{\lambda}{D_1}}, \quad 0 \leq p < \infty \quad (51)$$

$$H(r, p) \equiv \frac{J_0(rp)Y_0(ap) - J_0(ap)Y_0(rp)}{[J_0(ap)]^2 + [Y_0(ap)]^2}, \quad 0 \leq a \leq r, \quad 0 \leq p < \infty \quad (52)$$

$$G_1(z, p) \equiv \frac{\cosh\left(\frac{\mu_1 z}{\sqrt{D_1}}\right)}{\cosh\left(\frac{\mu_1 b}{\sqrt{D_1}}\right) + \frac{\mu_1}{\epsilon \mu_2} \left(\frac{D_1}{D_2}\right)^{\frac{1}{2}} \sinh\left(\frac{\mu_1 b}{\sqrt{D_1}}\right)}, \quad 0 \leq z \leq b, \quad 0 \leq p < \infty \quad (53)$$

$$G_2(z, p) \equiv \frac{\frac{\mu_1}{\epsilon \mu_2} \left(\frac{D_1}{D_2}\right)^{\frac{1}{2}} \sinh\left(\frac{\mu_1 b}{\sqrt{D_1}}\right) \exp\left[-\frac{\mu_2(z-b)}{\sqrt{D_2}}\right]}{\cosh\left(\frac{\mu_1 b}{\sqrt{D_1}}\right) + \frac{\mu_1}{\epsilon \mu_2} \left(\frac{D_1}{D_2}\right)^{\frac{1}{2}} \sinh\left(\frac{\mu_1 b}{\sqrt{D_1}}\right)}, \quad b \leq z < \infty, \quad 0 \leq p < \infty \quad (54)$$

$$I^i(r, z) = \int_0^{\infty} H(r, p) G_i(z, p) \Delta(p) p dp, \quad i=1,2 \quad (55)$$

for  $i=1, r \geq a, 0 \leq z \leq b$ ; for  $i=2, r \geq a, b \leq z < \infty$

With these notations we can write:

$$N_i(r, z) = N^* \left\{ \frac{K_0(\beta_i \frac{r}{a})}{K_0(\beta_i)} + (-1)^i \cdot \frac{2}{\pi} I^i(r, z) \right\}, \quad i=1,2 \quad (56)$$

for  $i=1, r \geq a, 0 \leq z \leq b$ ; for  $i=2, r \geq a, b \leq z < \infty$

Verification of Eqs.(49) and (50) is given in [10] Appendix C section 1.7.

#### 4.1. Mass Flux Derivation

We are also interested in the mass flux of species in the radial and axial directions. These quantities are given by:

$$j_1^r(r, z) = -D_1 \frac{\partial N_1(r, z)}{\partial r}, \quad r \geq a, \quad 0 \leq z \leq b \quad (57)$$

$$j_1^z(r, z) = -D_1 \frac{\partial N_1(r, z)}{\partial z}, \quad r \geq a, \quad 0 \leq z \leq b \quad (58)$$

$$j_2^r(r, z) = -\epsilon D_2 \frac{\partial N_2(r, z)}{\partial r}, \quad r \geq a, \quad b \leq z < \infty \quad (59)$$

$$j_2^z(r, z) = -\epsilon D_2 \frac{\partial N_2(r, z)}{\partial z}, \quad r \geq a, \quad b \leq z < \infty \quad (60)$$

Of particular interest is the mass flux on the cylinder surface, i.e., mass loss rate per unit surface area of infinite cylinder, which from Eqs.(49) and (50) and with the aid of Eqs.(55) and (56) is written as ([10], Appendix C section 1.8, Eqs.(C.66)-(C.69)):

$$j_1^r(a, z) = -D_1 \frac{\partial N_1(a, z)}{\partial r}, \quad 0 \leq z \leq b \quad (61)$$

$$= \frac{D_1 N^*}{a} \left[ \beta_1 \frac{K_1(\beta_1)}{K_0(\beta_1)} - \frac{4}{\pi^2} \int_0^\infty \Delta(p) G_1(z, p) \frac{p dp}{[J_0(ap)]^2 + [Y_0(ap)]^2} \right]$$

$$j_2^r(a, z) = -\epsilon D_2 \frac{\partial N_2(a, z)}{\partial r}, \quad b \leq z < \infty \quad (62)$$

$$= \frac{\epsilon D_2 N^*}{a} \left[ \beta_2 \frac{K_1(\beta_2)}{K_0(\beta_2)} + \frac{4}{\pi^2} \int_0^\infty \Delta(p) G_2(z, p) \frac{p dp}{[J_0(ap)]^2 + [Y_0(ap)]^2} \right]$$

Another quantity of interest is the rate of mass loss from a finite portion of the infinite cylinder which is equal to the height of the waste cylinder. The mass loss rate to the fissure and porous rock is given by:

$$\dot{m}_1 = 4\pi a \int_0^b j_1^r(a, z) dz \quad (63)$$

$$\dot{m}_2 = 4\pi a \int_b^{b+L} j_2^r(a, z) dz \quad (64)$$

where we have assumed the waste cylinder height to be  $2(b+L)$ . The result of substituting Eqs.(61) and (62) in Eqs.(63) and (64), respectively, and performing the integration is ([10], Appendix C section 1.9, Eqs.(C.70)-(C.75)):

$$\dot{m}_1 = 4\pi D_1 N^* \left[ b \beta_1 \frac{K_1(\beta_1)}{K_0(\beta_1)} - \frac{4}{\pi^2} \int_0^\infty \Delta(p) \frac{\sqrt{D_1}}{\mu_1} \right. \quad (65)$$

$$\left. \frac{\sinh\left(\frac{\mu_1 b}{\sqrt{D_1}}\right)}{\cosh\left(\frac{\mu_1 b}{\sqrt{D_1}}\right) + \frac{\mu_1}{\epsilon \mu_2} \left(\frac{D_1}{D_2}\right)^{\frac{1}{2}} \sinh\left(\frac{\mu_1 b}{\sqrt{D_1}}\right)} \frac{p dp}{[J_0(ap)]^2 + [Y_0(ap)]^2} \right]$$

$$\dot{m}_2 = 4\pi \epsilon D_2 N^* \left[ L \beta_2 \frac{K_1(\beta_2)}{K_0(\beta_2)} + \frac{4}{\pi^2} \int_0^\infty \Delta(p) \frac{\sqrt{D_2}}{\mu_2} \right. \quad (66)$$

$$\left. \frac{\frac{\mu_1}{\epsilon \mu_2} \left(\frac{D_1}{D_2}\right)^{\frac{1}{2}} \sinh\left(\frac{\mu_1 b}{\sqrt{D_1}}\right) [1 - \exp - \left(\frac{\mu_2 L}{\sqrt{D_2}}\right)]}{\cosh\left(\frac{\mu_1 b}{\sqrt{D_1}}\right) + \frac{\mu_1}{\epsilon \mu_2} \left(\frac{D_1}{D_2}\right)^{\frac{1}{2}} \sinh\left(\frac{\mu_1 b}{\sqrt{D_1}}\right)} \frac{p dp}{[J_0(ap)]^2 + [Y_0(ap)]^2} \right]$$

We assume that the mass loss rate from the cylindrical surface of a finite waste cylinder with the height  $2(b+L)$  is equal to:

$$\dot{m}_{total} = \dot{m}_1 + \dot{m}_2 \quad (67)$$

## 4.2. Numerical Demonstration

### 4.2.1. Method of Evaluation

Numerical results were obtained with the aid of a computer program. Since  $H(r, p)$  for  $a < r < \infty$ ,  $0 < p < \infty$  is an oscillatory function and has infinitely many zero roots, we write the concentration from Eq.(56) as:

$$N_i(r, z) = N^* \left\{ \frac{K_0(\beta_i \frac{r}{a})}{K_0(\beta_i)} + (-1)^i \cdot \frac{2}{\pi} \sum_{n=0}^{\infty} \Delta I_{\zeta_n}^i(r, z) \right\}, i=1,2 \quad (68)$$

for  $i=1, r \geq a, 0 \leq z \leq b$ ; for  $i=2, r \geq a, b \leq z < \infty$

where

$$\Delta I_{\zeta_n}^i(r, z) = \int_{\zeta_n}^{\zeta_{n+1}} H(r, p) G_i(z, p) \Delta(p) p dp, i=1,2, n=0,1,2,\dots \quad (69)$$

where  $\zeta_n$  is the  $n$ th zero of  $H(r, p)$ , and  $\zeta_0=0$ . The value of the integral between two successive zeroes is evaluated by the subroutine D01AJF from the NAG library [11]. D01AJF is a general-purpose integrator which calculates an approximation to the integral of a function  $F(x)$  over a finite interval (A,B):

$$\int_A^B F(x) dx$$

The routine can be used when the integrand has a singularity, especially when it is of an algebraic or a logarithmic type. The integration is stopped when the contribution from the  $n$ th interval is less than  $10^{-5}$  of the concentration.

The values of  $\zeta_n$  are determined first by estimating its magnitude by the following asymptotic result [ Eq.9.5.28 in Ref.9]:

$$\zeta_n \approx \frac{n \pi a}{\frac{r}{a} - 1}, n=1,2,\dots, r > a \quad (70)$$

and then using the C05AGF subroutine from the NAG library to get the exact result within a desired accuracy. C05AGF locates a simple zero of a continuous function from a given starting value, using first a binary search to locate an interval containing a zero of the function, then a combination of the methods of linear interpolation, extrapolation and bisection to locate the zero precisely within the desired accuracy which is an input to the subroutine. The subroutine also requires an interval as an input. The interval is used to bound the position of the zero root. The interval between successive zeros is almost known from Eq.(70). Therefore, the interval is so chosen to ensure that the same zero root is not encountered twice. The program (UCBNE-79) was executed on a VAX-8650 at Lawrence Berkeley Laboratory.

#### 4.2.2. Numerical Results

For a waste cylinder  $a = 15$  cm, we use  $D_1 = D_2 = 10^{-5}$  cm<sup>2</sup>/sec, where we have neglected the effect of tortuosity on  $D_2$ . Table 1 shows the values of  $\beta_1$  with  $K_1 = 1$  and  $\beta_2$  for some radionuclides of interest. Values of  $\beta_1$  and  $\beta_2$  are evaluated with the aid of Eq.(46A).

Figure 2 shows the variation of concentration at the fissure center line obtained from Eq.(49) with  $\frac{r}{a}$  for different  $\frac{a}{b}$  values. The  $\frac{a}{b} = 0$  curve indicates that the fissure width is infinite and the cylinder is exposed to ground water only. The  $\frac{a}{b} = \infty$  curve indicates that the cylinder is exposed to porous rock only, i.e., the fissure width is zero. One observes that the concentration is bounded by the above

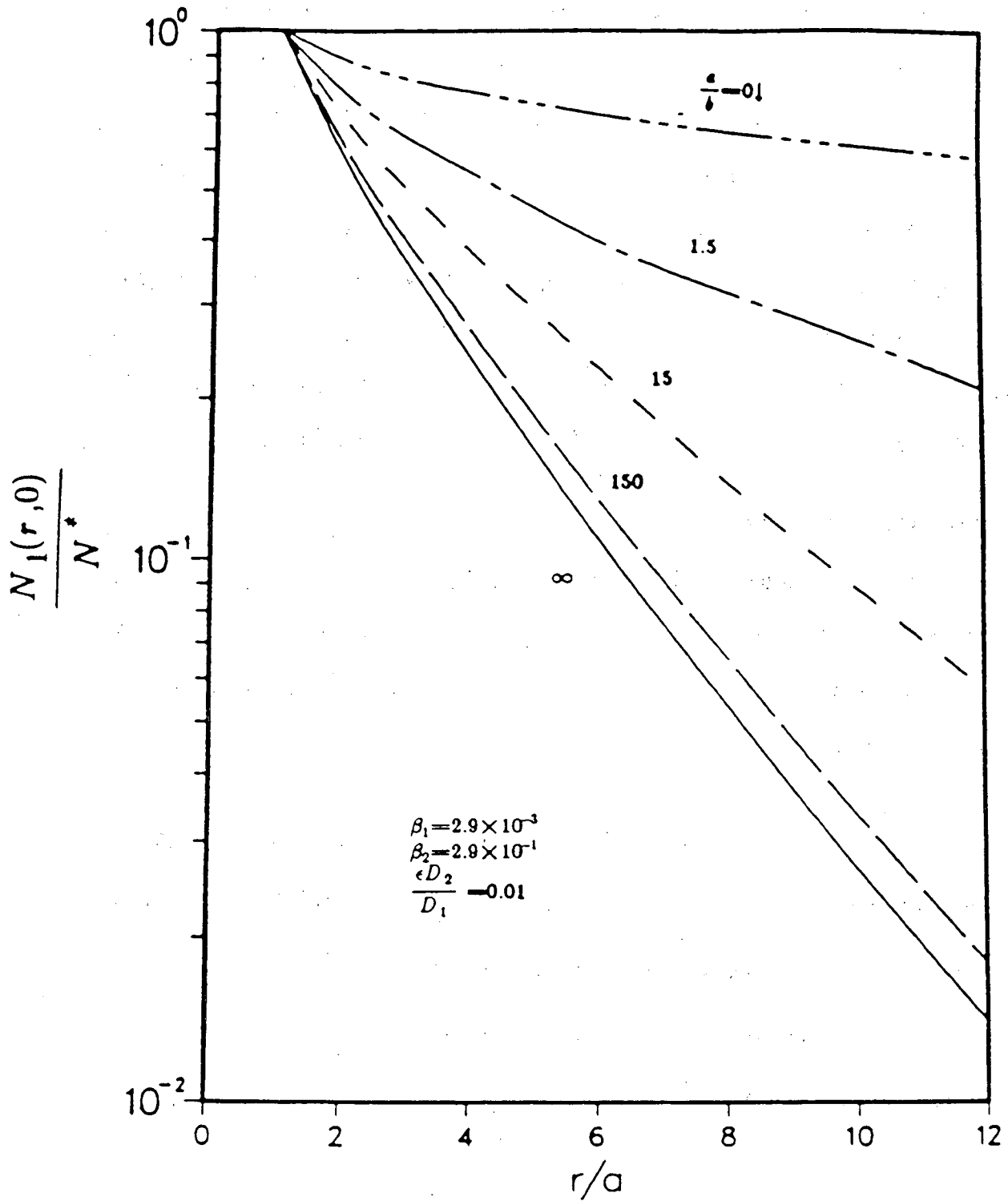


Figure 2 Variation of normalized concentration with  $r/a$  for different  $a/b$  ratios.

Table 5.1 Values of  $\beta_1$  and  $\beta_2$  for some radionuclides of interest.

Nuclide	Half-life, yr	$K_2^a$	$\beta_1$	$\beta_2$
Tc <sup>99</sup>	$2.12 \times 10^5$	5	$1.51 \times 10^{-3}$	$3.38 \times 10^{-3}$
U <sup>234</sup>	$2.47 \times 10^5$	50	$4.47 \times 10^{-4}$	$3.16 \times 10^{-3}$
Np <sup>237</sup>	$2.14 \times 10^6$	100	$4.78 \times 10^{-4}$	$4.78 \times 10^{-3}$
Pu <sup>242</sup>	$3.79 \times 10^5$	500	$1.14 \times 10^{-3}$	$2.55 \times 10^{-2}$
Am <sup>241</sup>	$4.58 \times 10^2$	500	$3.29 \times 10^{-2}$	$7.36 \times 10^{-1}$
Se <sup>79</sup>	$6.50 \times 10^4$	50	$2.74 \times 10^{-3}$	$1.94 \times 10^{-2}$
Sn <sup>126</sup>	$1.0 \times 10^5$	1000	$2.22 \times 10^{-3}$	$7.01 \times 10^{-2}$
Th <sup>230</sup>	$8.0 \times 10^4$	5000	$2.49 \times 10^{-3}$	$1.76 \times 10^{-1}$
Ra <sup>226</sup>	$1.6 \times 10^3$	500	$5.55 \times 10^{-3}$	$1.24 \times 10^{-1}$
C <sup>14</sup>	$5.73 \times 10^3$	10	$9.27 \times 10^{-3}$	$2.93 \times 10^{-2}$

a. Typical values of retardation coefficient in basalt

two extreme cases. The thinner a fissure is, the lower the concentration in the fissure.

For  $b=0.1$  cm and  $\frac{a}{b}=150$ , the concentration in the fissure is within few percent of

the concentration of  $\frac{a}{b}=\infty$ . Hence, for a waste cylinder and fissure width ( $\frac{a}{b} \gg 1$ )

one can approximate the concentration at the fissure center line by the concentration

of a radionuclide exposed to porous rock only, i.e.,  $\frac{a}{b}=\infty$ .

Figure 3 shows the variation of concentration of a long-lived radionuclide at the fissure center line with the normalized radial position  $\frac{r}{a}$  for different  $K_2$  values.

Here, we have chosen a fissure width of 2 cm, hence  $\frac{a}{b}=15$  and the concentration in the fissure is not within few percent of  $\frac{a}{b}=\infty$  (solid rock). As  $K_2$  increases the concentration in the fissure decreases. Because as  $K_2$  increases, the rock sorbs more nuclide and behaves as a stronger sink, hence extracting more nuclides from the fissure, which results in a decrease in the concentration.

Figure 4 shows the variation of the normalized concentration at the fissure's center line with the normalized radial position  $\frac{r}{a}$  for different  $\beta_1$  values. As  $\beta_1$  increases, more nuclides decay, resulting in a lower concentration. For a short-lived radionuclide the concentration drop is almost exponential with  $\frac{r}{a}$  as can be seen from Figure 4 for  $\beta_1=2.9 \times 10^{-2}$ . For a long-lived radionuclide the concentration variation is very gradual.

Figure 5 shows the variation of the concentration at 2 radii away with  $\frac{z}{b}$  for  $\frac{a}{b}=15$ . Also, the concentration far away from the fissure, i.e., as  $z \rightarrow \infty$  which is the asymptotic value is shown. One notes a flat concentration profile in the fissure. The concentration decreases as  $z$  increases beyond  $b$  and eventually will approach the asymptotic value. At  $\frac{z}{b}=26$  the concentration is within 5 percent of the asymptotic value. Therefore, for the parameters chosen here, the region of rock which is influenced by the fissure is about 26 cm. One can conclude that concentration profile in a rock with a single fracture is a good approximation for the concentration in a porous rock with multiple parallel fracture provided the distance between fractures is greater than 50 cm (for the parameters chosen here). If we had assumed that the

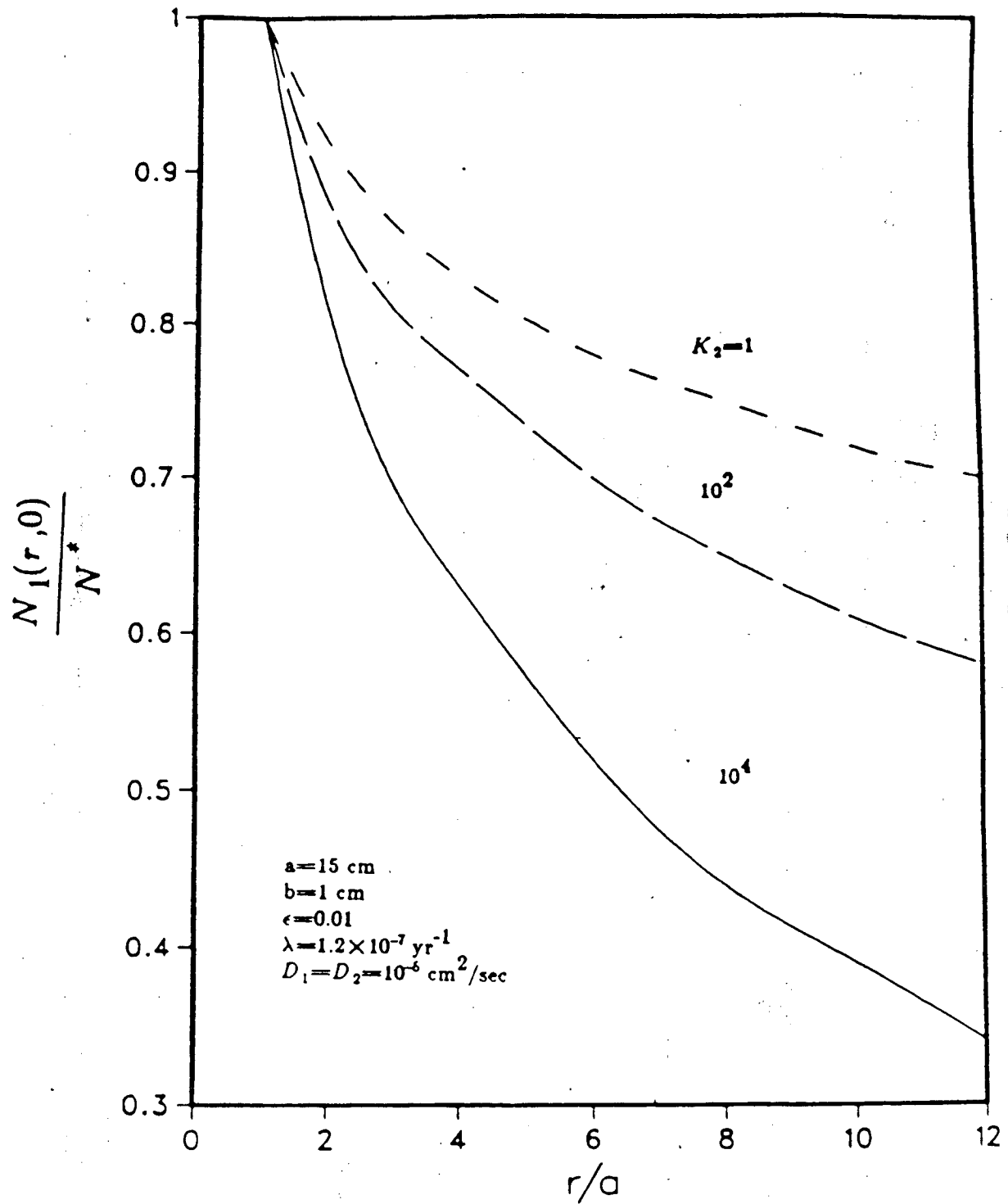


Figure 3 Variation of normalized concentration with  $r/a$  for different retardation coefficients.

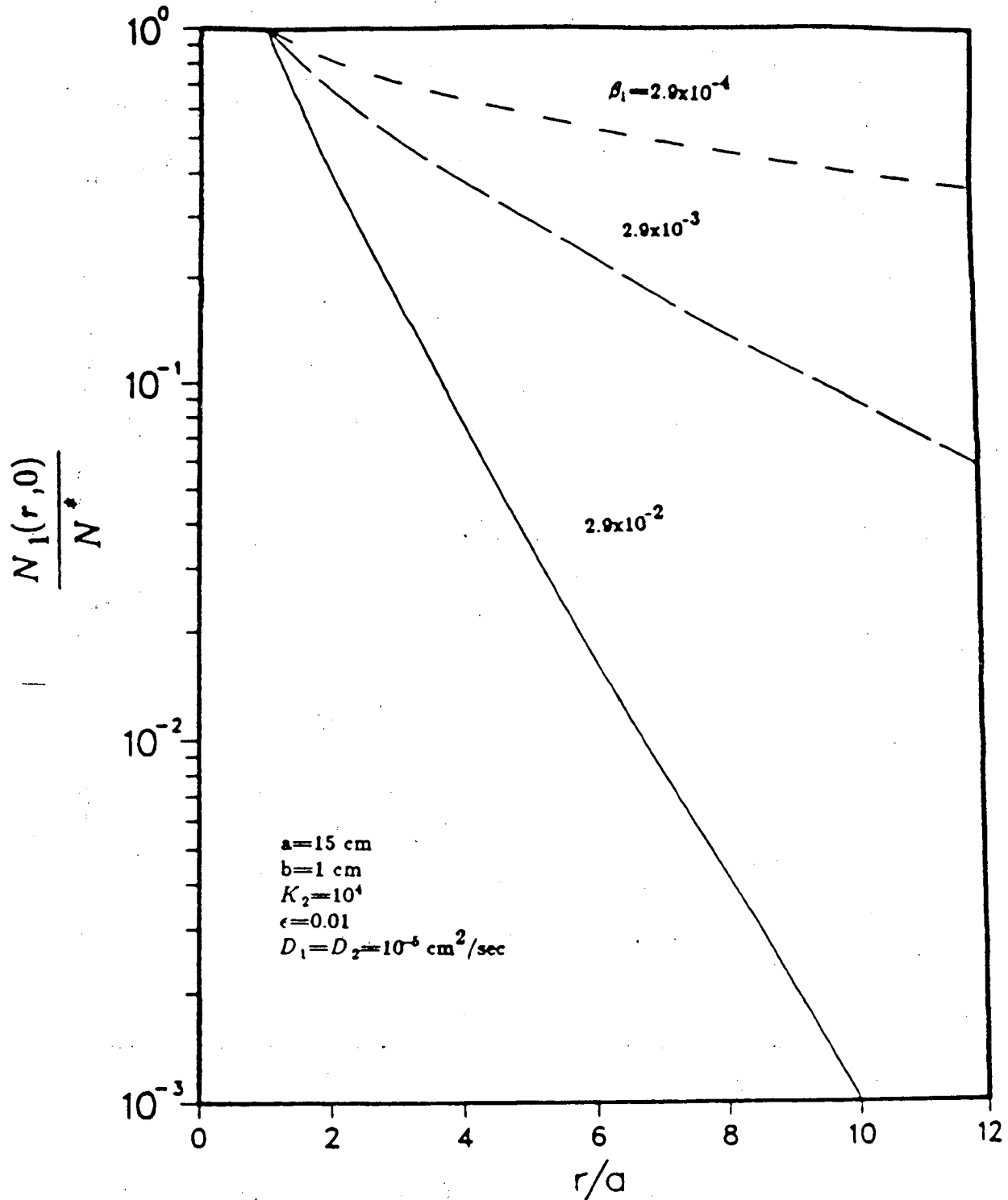


Figure 4 Variation of normalized concentration with  $r/a$  for different Thiele ( $\lambda$ ) values.

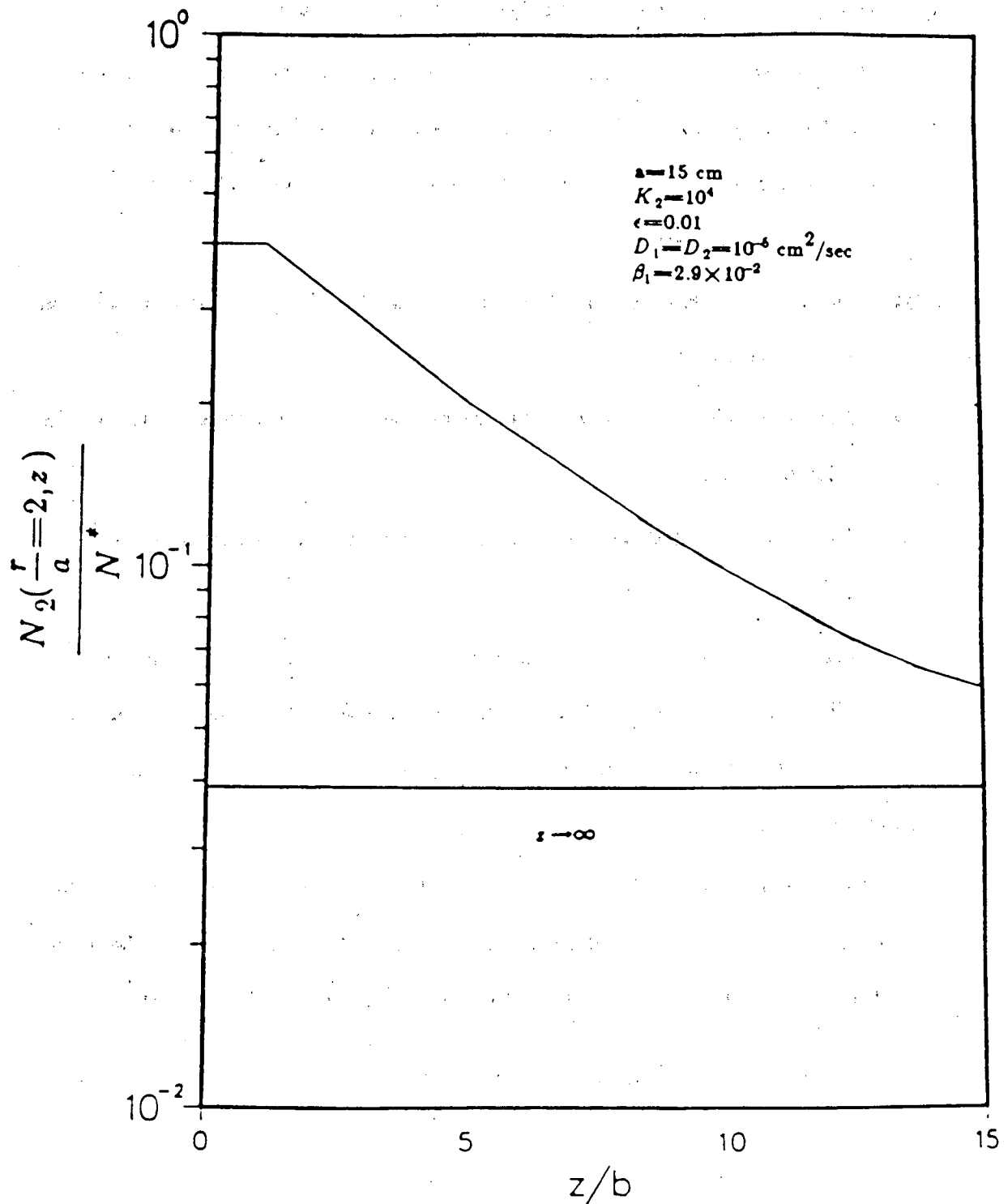


Figure 5 Variation of normalized concentration with  $z/b$  for  $a/b=15$ .

radionuclides do not diffuse in the radial direction in the porous rock then it would have followed that the concentration tends to zero as  $z \rightarrow \infty$ . Because the radionuclide would have decayed away by the time it would have diffused to  $z = \infty$ .

We have evaluated concentrations of different radionuclides in the fissure as a function of radial position. The numerical result indicates that the concentration in the fissure is almost uniform in the axial direction comparable to Figure 4. The following results were obtained:

- (1) The wider the fissure width becomes, the greater the concentration variation in the axial direction.
- (2) The larger the value of  $K_2$ , the greater the concentration variation in the axial direction.
- (3) The shorter the half life, the greater the concentration variation in the axial direction.

However, even for the most extreme case of  $K_2=10^4$ ,  $b=10$  cm, and the shortest-lived radionuclide from Table 1, numerical results show that the concentration at the fissure/rock interface is  $\geq 99.9$  percent of the concentration at the fissure's center line.

Before we proceed to give the numerical value of fluxes, we investigate the effect of porosity on mass flux. Consider the case where  $K_2=1$  (a non-sorbing nuclide), and  $D_1=D_2$ . Equation (51) yields  $\Delta(p)=0$ . From Eqs.(61) and (62) it follows that:

$$j_1(a, z) = \frac{N^* D_1}{a} \beta_1 \frac{K_1(\beta_1)}{K_0(\beta_1)} \quad 0 \leq z \leq b \quad (71)$$

$$j_2^r(a, z) = \epsilon \frac{N^* D_2}{a} \beta_2 \frac{K_1(\beta_2)}{K_0(\beta_2)} \quad b \leq z < \infty \quad (72)$$

Since  $\beta_1 = \beta_2$  it follows that the surface mass flux decreases by a factor of  $\epsilon$  across the interface.

Figure 6 shows the variation of surface mass flux with  $\frac{z}{b}$  for different  $\frac{a}{b}$  ratios. One observes that a thinner fissure has a higher mass flux, because the concentration is lower (see Figure 2) and the gradient is greater. Mass flux is almost uniform in the fissure and increases as the interface is approached, drops by a factor of  $\epsilon$  across the interface, and thereafter increases and approaches the asymptotic value ( $z \rightarrow \infty$ ). The asymptotic value is given by  $j_2^r(a, z)$  of Eq.(72). For  $\frac{a}{b} = 15$  after approximately 20 cm the asymptotic value is reached. One observes that due to porosity factor the mass flux into the fissure is greater than the mass flux into the porous rock.

Figure 7 shows the ratio of  $\frac{j_2^r(r, b)}{j_2^z(r, b)}$  for carbon-14 as a function of normalized radial position  $\frac{r}{a}$ . Numerical results show that more mass is transported in the radial direction on the porous side of the fissure than is diffused across the interface from fissure into the porous rock. At a distance of 2 radii away almost 200 times more mass is transported in the radial direction than the axial direction. The ratio increases as the waste surface is approached. On the waste surface the ratio is infinite due to uniformity of concentration with  $z$ , i.e.,  $j_z^2(r, b) = 0$ . Numerical results indicate that the radial diffusion in the porous rock is important and should not be excluded from fracture modeling as has been done by previous investigators.

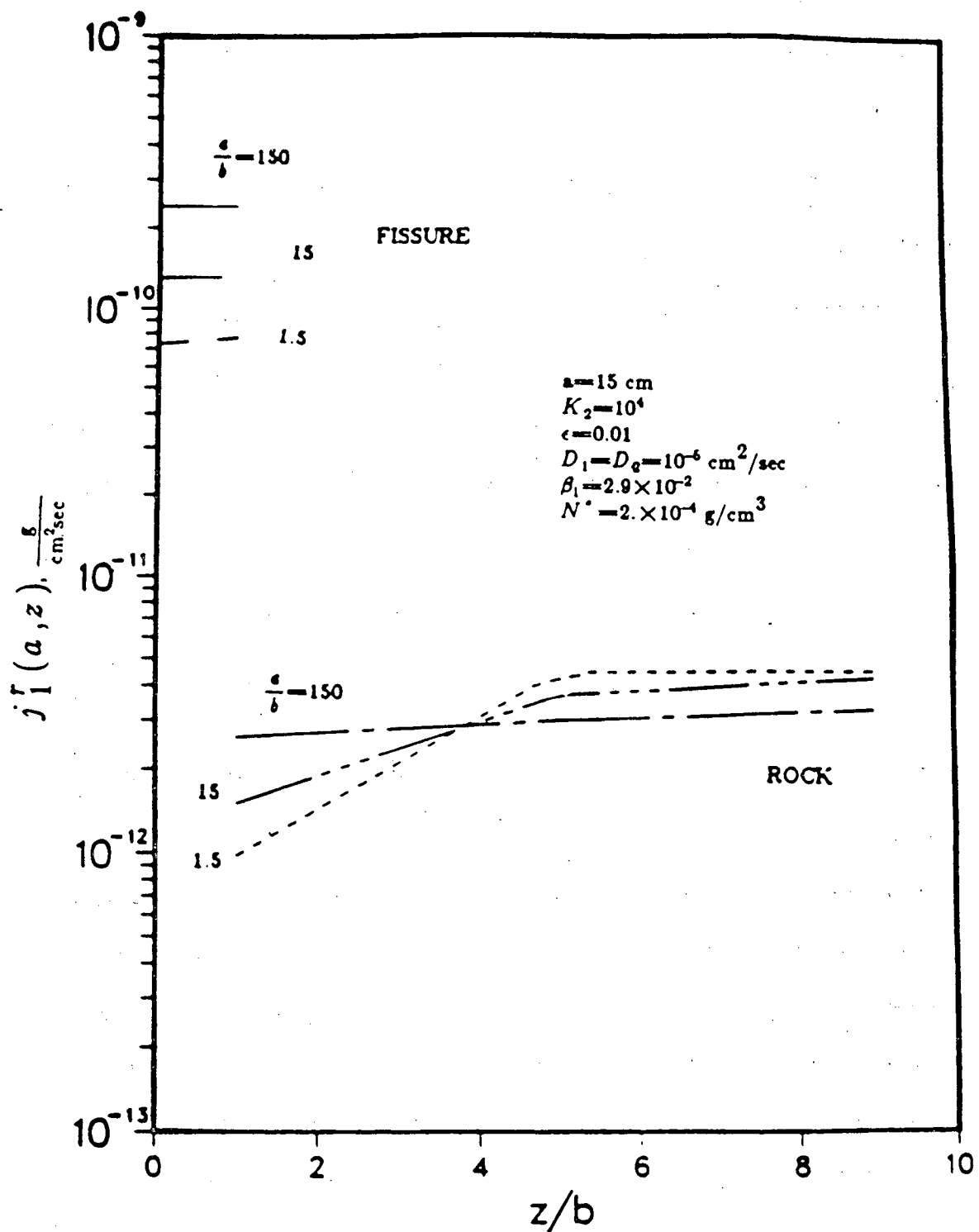


Figure 6 Variation of normalized flux with  $z/b$  for different  $a/b$  ratios. Note a drop across the interface is due to porosity factor.

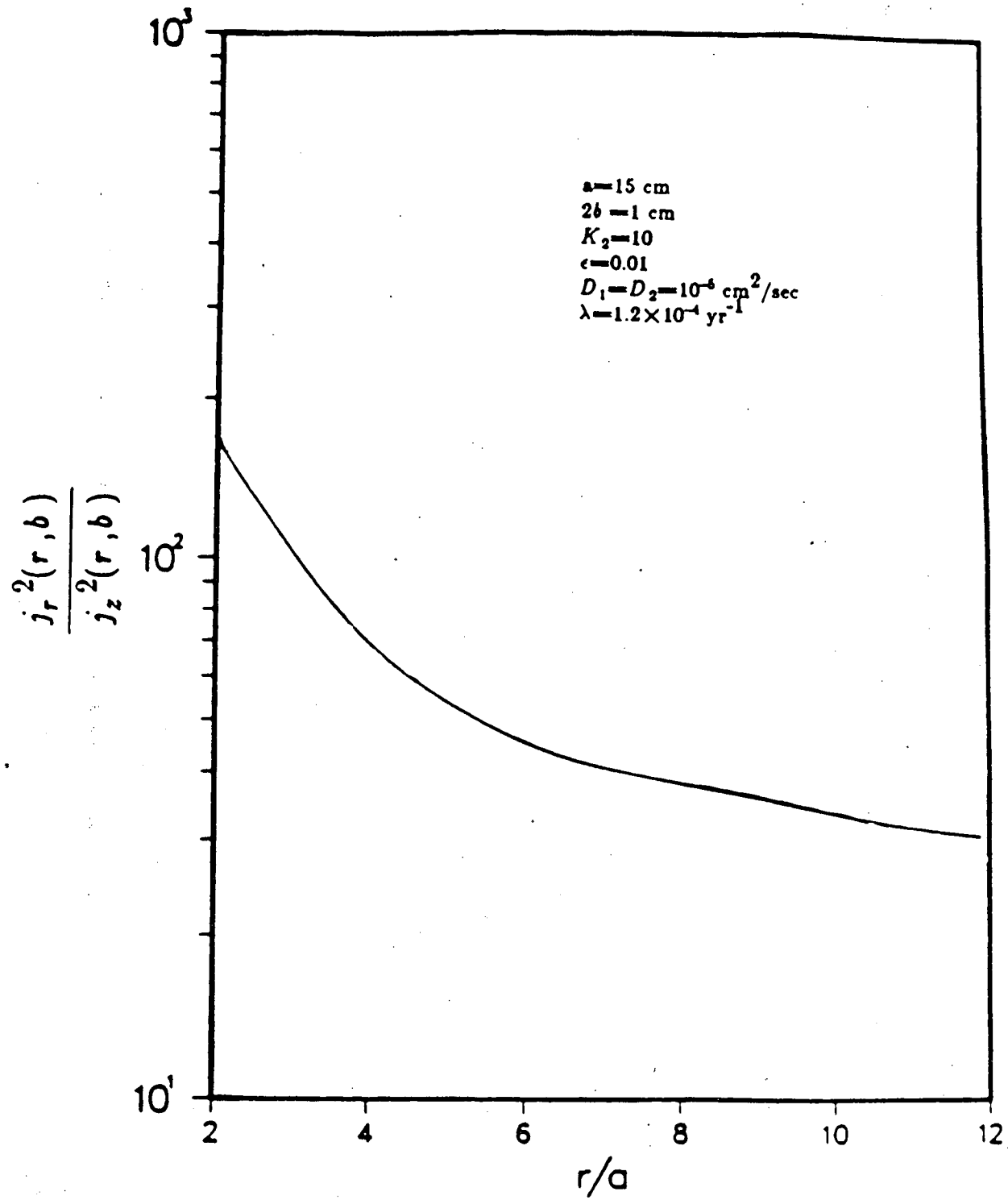


Figure 7 Ratio of mass flux in the radial direction to that in the axial direction at the rock/fissure interface.

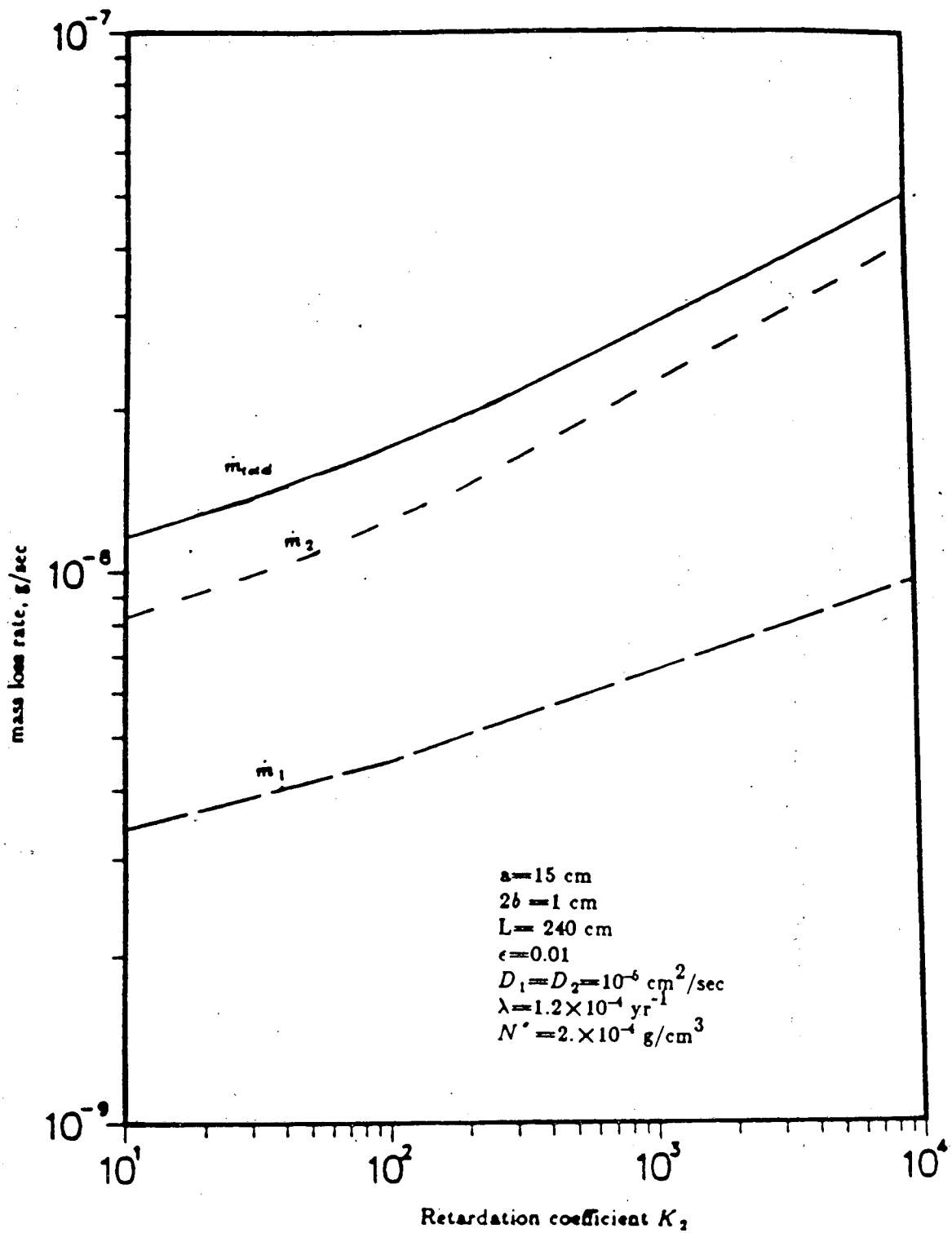


Figure 8 Variation of mass loss rate from a waste cylinder with retardation coefficient.

Figure 8 shows the mass loss rate of carbon-14 from a typical waste cylinder with a height of 240 cm, as a function of  $K_2$  values. A typical high-level waste glass cylinder has a height of 240 cm (Section 7.5 of Ref. [3]). The numerical value of parameters are shown on the figure; the saturation concentration is chosen to be equal to saturation concentration of vitreous silica and is for demonstration purpose only. The end effects are neglected. As  $K_2$  increases more nuclides are adsorbed by the porous rock, which results in a decrease in the concentration of the radionuclide in the porous rock (see Figure 3). As a result the concentration gradient in the radial and axial direction becomes steeper and the mass flux increases. It follows that more radionuclides diffuse from the fissure into the porous rock due to the steeper axial concentration gradient, which in turn results in a depletion of radionuclides in the fissure and an increase in the radial concentration gradient in the fissure. Data indicate that  $\dot{m}_2$  increases more rapidly with an increase in  $K_2$  than does  $\dot{m}_1$ . From Table 1,  $K_2=10$ , and from Figure 8 it follows that 3 times more mass is lost from the cylinder to the porous rock than from the cylinder to the fissure. Data indicate that neglect of radial diffusion in the porous rock underestimates the dissolution rate of waste considerably.

Here, we estimate the mass loss rate by making the following simplifications which are based on the numerical results (Figure 6).

- (1) Mass flux in the fissure is independent of  $z$  position and is equal to

$$\frac{N^* D_1}{a} \beta_1 \frac{K_1(\beta_1)}{K_0(\beta_1)}$$

- (2) Mass flux in the porous rock is independent of  $z$  position and is equal to the

asymptotic value, i.e.,  $\frac{\epsilon N^* D_2}{a} \beta_2 \frac{K_1(\beta_2)}{K_0(\beta_2)}$

It follows that:

$$\dot{m}_1^r(a, z) = 2\pi b N^* D_1 \beta_1 \frac{K_1(\beta_1)}{K_0(\beta_1)} \quad (73)$$

$$\dot{m}_2^r(a, z) = 2\pi \epsilon N^* D_2 L \beta_2 \frac{K_1(\beta_2)}{K_0(\beta_2)} \quad (74)$$

Using asymptotic values of  $K_0(x)$  and  $K_1(x)$  for small  $x$  [Eqs.(9.6.8) and (9.6.9) in Ref. 9], we obtain:

$$\dot{m}_1 = - \frac{2\pi b N^* D_1}{\ln(\beta_1)} \quad (75)$$

$$\dot{m}_2 = - \frac{2\pi L N^* D_2}{\ln(\beta_2)} \quad (76)$$

For carbon-14 using the values of  $\beta_1$ , and  $\beta_2$  given from Table 1 we calculate  $\dot{m}_1 = 2.7 \times 10^{-9}$  g/sec and  $\dot{m}_2 = 8.6 \times 10^{-9}$  g/sec. The exact values from Figure 8 are  $\dot{m}_1 = 3.4 \times 10^{-9}$  g/sec and  $\dot{m}_2 = 8.1 \times 10^{-9}$  g/sec.

## 5. Conclusions

The steady-state concentration of a diffusing nuclide from a waste cylinder has been obtained from the exact analytical solution. Here we investigate two phenomena which have been neglected by the previous investigators [1-5, 7]:

- (1) Effect of axial diffusion in the fissure.
- (2) Effect of radial diffusion in the porous rock.

Our numerical results indicate that, for a waste-cylinder radius of 15 cm and fissure width of 2 cm, one can neglect diffusion in the axial direction in the fissure, i.e., assume a uniform concentration in the axial direction. The steady-state concentration at the fissure/rock interface is  $\geq 99.9$  percent of the concentration at the fissure's center line. Hence, one can use the simplification introduced by [1]-[5] and

[7], i.e., concentration of the nuclide in the fissure in the transverse direction ( $z$  direction) is uniform.

On the other hand, radial diffusion in the porous rock is very important and should not be neglected as has been done in previous investigations. At steady-state about 3 times more mass is lost from the waste cylinder to the rock than is lost to the fissure. Furthermore, results indicate that close to the waste cylinder approximately 100 times more mass is transported in the radial direction in the porous rock adjacent to the fissure than is diffused across the fissure/rock interface. Therefore, neglect of radial diffusion in the porous rock will cause underestimation of the dissolution rate.

## 6. References

1. Grisak, G. E., J. F. Pickett, " Solute Transport Through Fractured Media 1. The Effect of Matrix Diffusion", *Water Resources Research*, 16, 719-730, (1980).
2. Neretnieks, I., "Diffusion in the Rock Matrix, An Important Factor in Radionuclide Retardation", *J. Geophys. Res.*, 85B, 4379, (1980).
3. Chambre', P. L., T. H. Pigford, A. Fujita, T. Kanki, R. Kobayashi, H. Lung, D. Ting, Y. Sato, and S.J. Zavoshy, " Analytical Performance Models for Geologic Repositories", LBL 14842, Vol. 2, (1982).
4. Tang, D. H., E. O. Frind, E. A. Sudicky, "Containment Transport in Fractured Porous Media: Analytical Solution for a Single Fracture", *Water Resources Research*, 17, 555-564, (1981).
5. Lever, D. A., M. H. Bradbury, S. J. Hemingway, "Modelling the Effect of Diffusion into the Rock Matrix on Radionuclide Migration", *Progress in Nuclear Energy*, 12, 85-117, (1983).
6. Chambre', P. L., personal communication.
7. Sudicky, E. A., E. O. Frind, "Containment Transport in Fractured Porous Media: Analytical Solutions for a System of Parallel Fractures", *Water Resources Research*, 18, 1643, (1982).
8. Griffith, James L., "On Weber Transforms", *J. Proc. Roy. Soc. N. S. Wales*, 89, 232-248, (1956).

9. Abramowitz, M., I. A. Stegun, *Handbook of Mathematical Functions with Formulas, Graphs, and Mathematical Tables*, National Bureau of Standards, Applied Mathematics Series, 55 , 3rd printing, (1965).
10. Zavoshy, S. J., "A Glass Dissolution Model and Mass Transfer from a Waste Glass Cylinder Intersected by a Fissure," Dissertation, University of California, (1987).
11. NAG library, *Numerical Algorithm Group*, 1101 31st Street, Suite 100, Downers Grove, Illinois, (1984).

LAWRENCE BERKELEY LABORATORY  
TECHNICAL INFORMATION DEPARTMENT  
UNIVERSITY OF CALIFORNIA  
BERKELEY, CALIFORNIA 94720